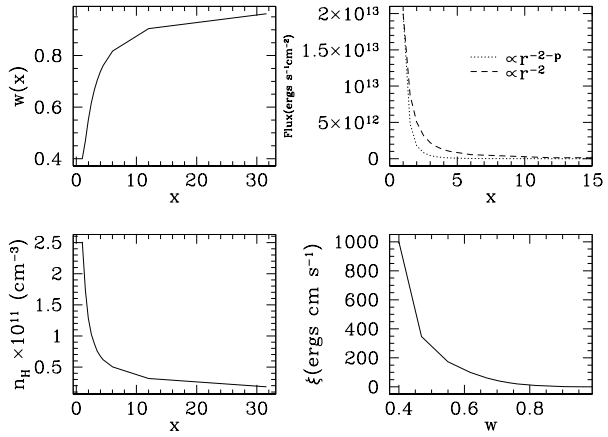

Fig. 6. Variation of the main kinematic and ionization variables for model B (see text). Upper left: Velocity law $w(x)$ for the model. Upper right: The ionizing radiative flux, decaying as $\propto r^{-2}$ (dashed line) and as $\propto r^{-2-p}$ (dotted line). Lower left: Variation of the density as function of x. Lower right: Variation of the ionization parameter (ξ) with the normalized velocity.

TABLE 2

COMPOSITION AND PARAMETER VALUES OF THE KINEMATIC MODEL B[a]

Element	Relative Abundance
H	1.0
He	0.1
C	0.3540E-03
N	0.9330E-04
O	0.7410E-03
Ne	0.1200E-03
Mg	0.3800E-04
Si	0.3550E-04
S	0.2140E-04
Ar	0.3310E-05
Ca	0.2290E-05
Fe	0.3160E-04

[a]In this model $w_0 = 0.4$, $v_\infty = 1100$ km s^{-1}, $\log_{10} r_0 = 15.75$ [cm], $v_{\rm turb} = 200$ km s^{-1} and $N_H = 5\times10^{20}$ cm^{-2}.

$\log n_H = 11.40 - 10.26$ [cm^{-3}]. We compare models A and B in terms of the variation of optical depth vs. velocity of the flows of three important lines, i.e, Si XIV λ6.182, Si XIII λ6.648 and Mg XII λ7.106. We could estimate the contribution of each cloud to the formation of the composite profiles of these lines. We note that model B is superior to model A in describing the low-velocity portion of the flow reflected by the high ionization lines seen in NGC 3783 (extended blue wings), but yields a worse description of the spectrum at the higher terminal velocities responsible for the center of the lines measured by Kaspi et al. (2002).

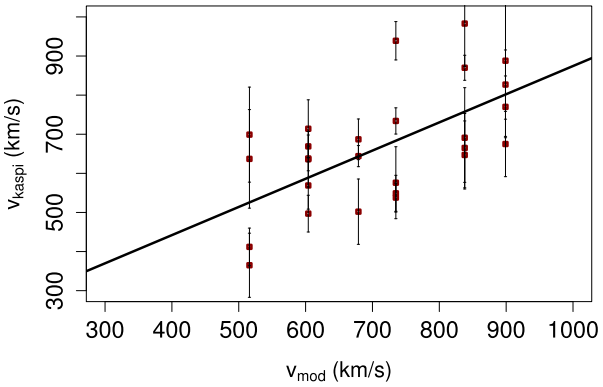

Fig. 7. Measured vs model predicted velocities for the group of unblended lines given in Table 2 of Ramírez et al. (2005). The measurements are taken from Kaspi et al. (2002). The solid line is the best line after a linear regression for model B.

Figure 7 shows the fit of a linear model by robust regression using the M estimator for model B. As in model A, the weights are included as the inverse of the variances, with the variance equal to $\Delta v = (v_{\rm lo} + v_{\rm hi})/2$, and $v_{\rm lo}$, and $v_{\rm hi}$ are the differences between centroid and the lower and upper velocity limits of the measured lines given in Table 3 of Kaspi et al. (2002). The best-fit slope is 0.72 ± 0.20 (solid line in the figure), and the residual standard error (rms) is 17.6 for 25 degrees of freedom (dof). In general, the scatter becomes worse for lines with terminal velocities greater than 1100 km s^{-1}.

5.1. *Modeling global properties - ξ vs velocity*

One of the prime goals of this study is to examine the relationship between the kinematics and the ionization structure of the flow. This is complementary to earlier work (Krongold et al. 2003; Netzer et al. 2003; Krongold et al. 2005) which follows the algorithm of constructing a grid of static photoionization models, with varying ionization parameter and column density, with the selection of this quantities which best reproduce the EW observed in the spectra, in addition to paying attention to the relationship between these physical parameters and the position in wavelength space of the absorption troughs.

Krongold et al. (2003) fitted photoionization models to the 900 ks spectrum of NGC 3783 using